Journal Pre-proof

The dominant influencing factors of desertification changes in the source region of Yellow River: Climate change or human activity?

Bing Guo, Cuixia Wei, Yang Yu, Yifeng Liu, Jialin Li, Chao Meng, Yumei Cai

Please cite this article as: B. Guo, C. Wei, Y. Yu, et al., The dominant influencing factors of desertification changes in the source region of Yellow River: Climate change or human activity?, *Science of the Total Environment* (2021), https://doi.org/10.1016/j.scitotenv.2021.152512

This is a PDF file of an article that has undergone enhancements after acceptance, such as the addition of a cover page and metadata, and formatting for readability, but it is not yet the definitive version of record. This version will undergo additional copyediting, typesetting and review before it is published in its final form, but we are providing this version to give early visibility of the article. Please note that, during the production process, errors may be discovered which could affect the content, and all legal disclaimers that apply to the journal pertain.

The Dominant Influencing Factors of Desertification Changes in the Source Region of Yellow River: Climate Change or Human Activity?

Bing Guo[1,2,3,4,5,6,7*], Cuixia Wei[1,*],Yang Yu[1,*],Yifeng Liu[1],Jialin Li[1],Chao Meng[3], Yumei Cai[3]

[1] School of Civil Architectural Engineering, Shandong University of Technology, Zibo 255000, Shandong, China;

[2] Key Laboratory of Meteorology and Ecological Environment of Hebei Province，Shijiazhuang 050021，Hebei，China;

[3] Key Laboratory of Land use, MNR, China Land Survey and Planning Institute, Beijing, 100035, China;

[4] Key Laboratory of Digital Earth Science, Chinese Academy of Sciences, Beijing 100101, China;

[5] State Key Laboratory of Resources and Environmental Information System, Institute of Geographic Sciences and Natural Resources Research of Chinese Academy of Sciences, Beijing 100101, China;

[6] Key Laboratory of Urban Land Resources Monitoring and Simulation, Ministry of Natural Resources, Shenzhen 518000, China；

[7] Key Laboratory of National Geographic Census and Monitoring, Ministry of Natural Resources, Wuhan 430072, China;

Corresponding Author:

Bing Guo Cuixia Wei Yang Yu

Xincun West road 266, Zhangdian District, Zibo 255000 , China

Tel.: +86 18766965987；+8617853318457；+8618766965782

Email:guobingjl@163.com；1461521281@qq.com; 1565548173@qq.com

Abstract: Due to the combined effects of global warming and human activities, the ecological environment of the Yellow River source area has undergone profound changes and desertification has become increasingly prominent. In this study, an optimal desertification monitoring index based on feature space was proposed for the Yellow River source area, and constructed using Landsat images. Then, the spatial and temporal variation of desertification in the Yellow River source area and its driving mechanism were studied using Geodetector. The main conclusions are as follows: (1) The newly proposed feature space-based desertification monitoring index has good applicability in the study area. The best inversion accuracy of the point-to-point Albedo-NDVI feature space model was 88.4 %. (2) Desertification in the eastern and southern regions of the Yellow River source area has a tendency to increase, while the desertification situation in the central region is relatively stable. (3) From 1995 to 2015, there was a significant improvement in desertification in the study area, as evidenced by a decrease in desertification intensity. (4) As the intensity of human disturbance increases, the influence of natural factors on desertification gradually diminishes. The interaction of natural and anthropogenic factors has greater explanatory power for desertification than that of individual natural or anthropogenic factors. The research results can be used as a reference for decision-making on desertification control in the Three-River Source Region.

Keywords: Desertification; Feature space; Spatial and temporal pattern; Geodetector; Source region of Yellow River.

1. Introduction

Land desertification is characterized by wind and sand activities in semi-arid, arid and

partially semi-humid zones due to excessive exploitation and utilization of land (Zhao et al., 2009; Guo et al., 2020a). Due to unreasonable anthropogenic disturbances such as grassland reclamation, continuous cultivation and overgrazing, as well as global climate change, the desertification situation in the Three River Source Region, especially in the source area of the Yellow River, is becoming increasingly prominent (Li et al., 2011). In addition, deforestation and desertification caused by human activities and climate change pose a major challenge to sustainable development and affect the lives and livelihoods of millions of people. Dynamic monitoring of desertification is essential to improve regional livelihoods, reduce vulnerability and mitigate economic risks (SDGs 15: Life and land). Meanwhile, climate change is becoming a prominent factor affecting land degradation processes, causing significant damage to regional sustainable development and economies. Therefore, it is urgent to reveal the mechanisms of climate change and human activities on desertification for the protection and restoration of regional ecosystems (SDGs 15: Climate action).

In the past decades, many scholars at home and abroad have conducted studies on remote sensing monitoring of desertification or vegetation degradation in the Yellow River source area and its surrounding areas. Yan et al. (2009) utilized image interpretation techniques and based on Landsat MSS and TM data to obtain information on windsanding in Longyangxia Reservoir, upper Yellow River, China, and then analyzed the driving factors. Ma et al. (2013) utilized the image datasets of AVHRR, MODIS, and Landsat TM to dynamically monitor the desertification and found that Landsat TM data are better applicable in monitoring desertification in small areas with appropriate spatial and temporal resolution. Shen et al. (2018) studied the degradation and recovery of vegetation in the Three-River Source Region from 2000 to 2015 based on MODIS

NDVI and the impact of ecological protection projects, and found that the vegetation showed an

overall recovery and ecological protection projects had a positive effect on vegetation recovery.

Zhang et al. (2018) used Landsat images from 1977-2015 to establish a new classification system

for weathered land in the highlands, and then applied the system to obtain the spatial distribution

of desertification through visual interpretation. Zheng et al. (2018) developed a series of pixel

based vegetation dynamics stepwise-cluster prediction models to establish the relations between

NDVI and climate conditions in Three-River Source Region and then predicted the future spatial

and temporal distribution of vegetation coverage in 2020, 2040, 2060, 2080, and 2100. Sun et al.

(2019) studied the change process of grassland desertification in Northern Tibet (including the

Yellow River source area) using NDVI and landscape index, and found that the overall

improvement in grassland condition was smaller than the restored area during 2001-2015. Zhang

and Jin (2021) utilized the MODIS NDVI images to investigate the spatiotemporal changes in

vegetation degradation and restoration in Three-River Source Region (Yellow River, Lancang

River, and Yangtze River) and then quantitatively identified the contributions of climate change

and anthropogenic factors. However, most of the above studies applied the single indices (such as

NDVI) or image classification method to detect or monitor the spatial and temporal change of

desertification. Due to the fact that the evolution process of desertification was always

interactively influenced by natural and anthropogenic factors, the single index method could not

better identify the information of desertification. Similarly, image classification methods can only

determine the spatial extent of desertification and cannot obtain quantitative information.

In recent years, feature space model that could consider the interactions between the two

factors had been utilized to monitor drought and soil salinization. Feng et al.(2018) proposed the

Albedo-MSAVI feature space model in which the normalized difference vegetation index (NDVI) was replaced by modified soil adjusted vegetation index (MSAVI) and found that the inversion accuracy of improved model of soil salinization model had been greatly improved than that of previous model. Guo et al. (2020c) introduced five typical surface parameters(surface Albedo, vegetation index, salinity index, humidity index, and Iron oxide index) to propose an salinization minoring index of Yellow River Delta based on feature space. However, fewer studies about desertification based on feature space were reported. Huete et al. (1988) introduced MSAVI to indicate the desertification condition to avoid the impacts of soil vegetation background, which took complete account of the fundamental soil line problem. Zeng et al. (2005) established the difference index model of desertification monitoring by investigating the relationships between NDVI, Land Surface Temperature (LST), and desertification index. Lamchin et al. (2016) used NDVI, TGSI and surface Albedo to reflect surface conditions such as vegetation biomass, landscape pattern and micrometeorological indices, respectively, and found significant relationships between TGSI and Albedo in indicating desertification conditions. Liu et al. (2018) found that different degree of desertification could lead to differences in topsoil texture and then applied the topsoil grain size index (TGSI) to evaluate the condition of land degradation. However, the above studies on desertification are primarily based on a single index, image classification, or comprehensive index method to extract desertification information. At the same time, the interaction of several types of surface parameters in the desertification process has been ignored (Guo et al., 2020e).

In this study, five typical indices of desertification were obtained based on Landsat images and then introduced to construct ten feature space models. Then the optimal desertification

monitoring index based on remote sensing and feature space model in the source region of Yellow

River was constructed and established. Additionally, the temporal and spatial change patterns of

desertification and the dominant influencing factors of the desertification changes were explored

and discussed.

2. Materials and Methods

2.1. Study Area

The source region of Yellow River (95°52′-99°29′E，35°42′-35°20′N (Fig.1)) is

located on the northeast edge of the Qinghai-Tibet Plateau and is an integral part of the

Three-River Source Region. The study region is mainly composed of plateau plains, mountains,

and hilly platforms (Wu et al., 2021). The average elevation is 4029 m and the topography is

undulating, ranging from 2585 m in the eastern region to 6253 m in the western region (Li et al.,

2011). Furthermore, the climate in the study area is of the semi-arid and alpine climate types,

with typical inland plateau climate characteristics. The precipitation is scare and concentrated, its

average value is 312 mm, while the average annual temperature is below -4 °C. Affected by

topography, the temperature and precipitation in the study region decreased from east to west

(Zeng et al., 2007; Yuan et al., 2015; Zhang et al., 2021). The eco- environmental problems have

become prominent in some alpine regions as a result of its unique topography and the influence

of alpine climate, as well as natural disturbance and human activities in the study region, such as

grassland degradation, the disorder of grassland ecosystem function, reduction of lakes and
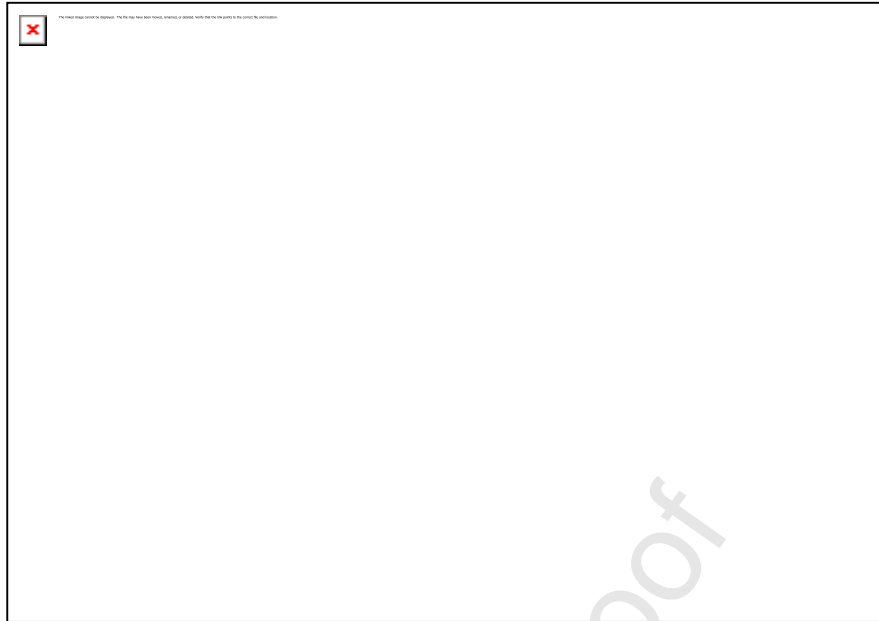
wetlands, and weakening of water conservation.

Fig. 1. Location of the study area and its topographic features.

2.2. Data source

The images of Landsat TM/OLI are downloaded from the geospatial data cloud platform (available at http://www.gscloud.cn/), with a temporal and spatial resolution of 16 days and 30 m. The path/row of the images ranges from 132 to135 and 35 to 37, respectively. A total of 33 images for 1995 (1994-1996), 2005 (2004-2006), and 2015 (2014-2016) (11 images for each year) with the cloud cover less than 10% have been collected during the growing season, especially in July and August. The above images were then geometrically corrected and atmospherically corrected for the FLAASH model using ENVI 5.3. Datasets of land use (1:100000), GDP density (1km) , and population density (1km) are all obtained from the Resource and Environment Science and Data Center (RESDC, available at https://www.resdc.cn/). Meteorological station data, including daily average temperature and daily precipitation are downloaded from National Meteorological Science Data Center (http://data.cma.cn/). The datasets of vegetation types with a scale of 1:1000000 are also obtained from RESDC，which are composed of 54 vegetation types, including deciduous shrubs, shrubs, evergreen coniferous forest, grasslands, and meadows.

2.3. Methods

2.3.1. Principle of Feature Space

Feature space is convenient approach to monitor the soil moisture, drought, and soil salinity, which is composed of two typical surface parameters that derived from satellites images (Zeng et al., 2006; Ren et al., 2014; Guo et al., 2020a). It has provided a better reference for monitoring the desertification. NDVI can reflect the spatial distribution intensity of aboveground plant, which can better indicate the growth status of plants (Wen et al., 2020). The NDVI would decrease with the intensified desertification. Thus, NDVI can be applied to evaluate the degree of desertification. Whereas the surface albedo (Albedo) determines the amount of radiation that absorbed by the underlying surface (Ren et al., 2014). The changes of the surface albedo will be affected by vegetation coverage, water, soil moisture, and snow cover (Zeng et al., 2006). The albedo will increase with the aggravation of desertification that leads to the decreased surface water and surface roughness. The Albedo-NDVI feature space has been established by considering Albedo as the ordinate and NDVI as the abscissa. As shown in Fig. 2, there is a nonlinear relationship between Albedo and NDVI. The upper boundary line A-D line refers to the high-Albedo line, which indicates the maximum value of Albedo under certain vegetation coverage. The lower boundary line B-C line refers to the low line of Albedo, which demotes the minimum value of Albedo under given vegetation coverage. The constructed feature space has been enclosed by A, B, C, and D, which contains all the ground objects and shows better spatial distribution rule (Pan et al., 2010).
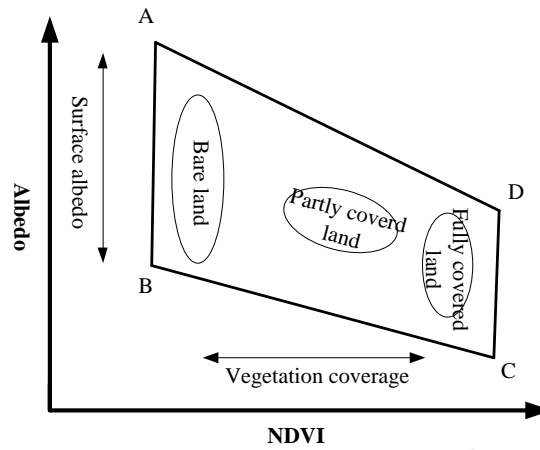
Fig.2. Principle of Feature Space (Taking Albedo NDVI as example).

2.3.2. Geodetector Model

Spatial differentiation is one of the basic characteristics of geographical phenomena. The Geodetector is an effective approach to detect spatial differentiation and better reveal and determine the dominant driving force (Wang et al., 2017). The core concept of this above method is that there would be obvious similarity between the above variables in spatial distribution, while a dependent variable is significantly influenced by an independent variable. The Geodetector is composed of four detectors, namely Ecological detector, Differentiation and Factor detector, Risk area detector, Interaction detector. The Differentiation and Factor detector; and Interaction detector have been applied in this paper. The Differentiation and Factor detector can explore and determine what extend a factor X explains the spatial differentiation of Y. In addition, the influence of factor X on factor Y can be measured by q value and its formulas are as follows.

$$q = 1 - \frac{N_h}{N} = 1 - \frac{\text{SSW}}{\text{SST}} \tag{1}$$

$$q = 1 - \frac{\sum N_h \sigma_h^2}{N \sigma^2} = 1 - \frac{\text{SSW}}{\text{SST}} \tag{2}$$

$$\text{SSW} = \sum_{h=1}^{L} N_h \sigma_h^2 \qquad\qquad (3)$$

$$\text{SST} = N\sigma^2 \qquad\qquad (4)$$

Where N_h refers to the number of units in layer h; H represents the stratification or classification of variable Y or factor X (1, …, L); σ^2 refers to the variance of y value of the whole region; N represents the unit number of the whole region; σ_h^2 represents the variance of the Y value of layer h; SST and SSW refers to the whole regional variance and the sum of intra-layer variance and, respectively. The value of q ranges from 0 to 1. the larger the value, the higher explanatory power of X for the spatial differentiation of Y (Zhu et al., 2018).

Interaction detector can distinguish and determine the interaction types between different factors X_i on Y, that is, evaluate whether the joint action of factors X_1 and X_2 will strengthen or weaken the explanatory power of dependent variable Y, or whether their influences on Y are independent from each other.

3. Construction of desertification remote sensing monitoring model based on feature space

3.1 Calculation of typical surface parameters

Based on fully considering the ecological environment characteristics of desertification in the study area, five typical surface parameters of desertification were selected in this study (Fig.3, taking Maduo County as example): NDVI, MSAVI, TGSI, Albedo and LST. Furthermore, the quantitative inversion was carried out based on the surface reflectance of Landsat images (after atmospheric correction with FLAASH model) utilizing ENVI 5.3 and the formulas(5)-(8) are expressed as follows(Zeng et al., 2006; Feng et al., 2018; Guo et al., 2020a).

$$\text{NDVI} = (B_{\text{NIR}} - B_{\text{RED}}) / (B_{\text{NIR}} + B_{\text{RED}}) \tag{5}$$

$$\text{MSAVI} = (2B_{\text{NIR}} + 1 - \sqrt{(2B_{\text{NIR}} + 1)^2 - 8(B_{\text{NIR}} - B_{\text{RED}})}) / 2 \tag{6}$$

$$\text{TGSI} = (B_{\text{RED}} - B_{\text{BLUE}}) / (B_{\text{RED}} + B_{\text{BLUE}} + B_{\text{GREEN}}) \tag{7}$$

$$\text{Albedo} = 0.356B_{\text{BLUE}} + 0.13B_{\text{RED}} + 0.373B_{\text{NIR}}$$
$$+ 0.085B_{\text{SWIR}_1} + 0.072B_{\text{SWIR2}} - 0.0018 \tag{8}$$

Where B_{NIR}, B_{RED}, B_{BLUE}, B_{GREEN}, B_{SWIR1}, and B_{SWIR2} refer to the surface reflectance of near infrared band, red band, blue band, green band, short wave infrared band, respectively.

The formulas(9)-(11) for land surface temperature (LST) are as follows (Li, 2020; Wen et al., 2020; Wu et al., 2021).

$$\text{LST} = a(1 - C - D) + (b(1 - C - D) + C + D)T_{10} - DT_a \tag{9}$$

$$C = \tau\varepsilon \tag{10}$$

$$\text{D} = (1 - \tau)[1 + (1 - \varepsilon)\tau] \tag{11}$$

Where LST refers to the land surface temperature; a, b is coefficient (a=-67.35535, b=0.458608), ε represents the surface emissivity, τ refers to the atmospheric transmittance, T_{10} refers to the radiance temperature of thermal infrared B_{10}(K) of Landsat8 TIRS, ☒ is the atmospheric average temperature.
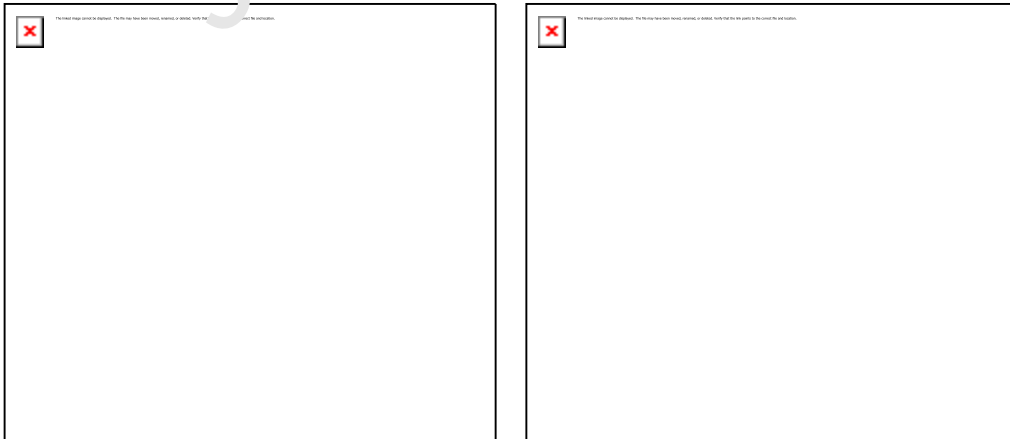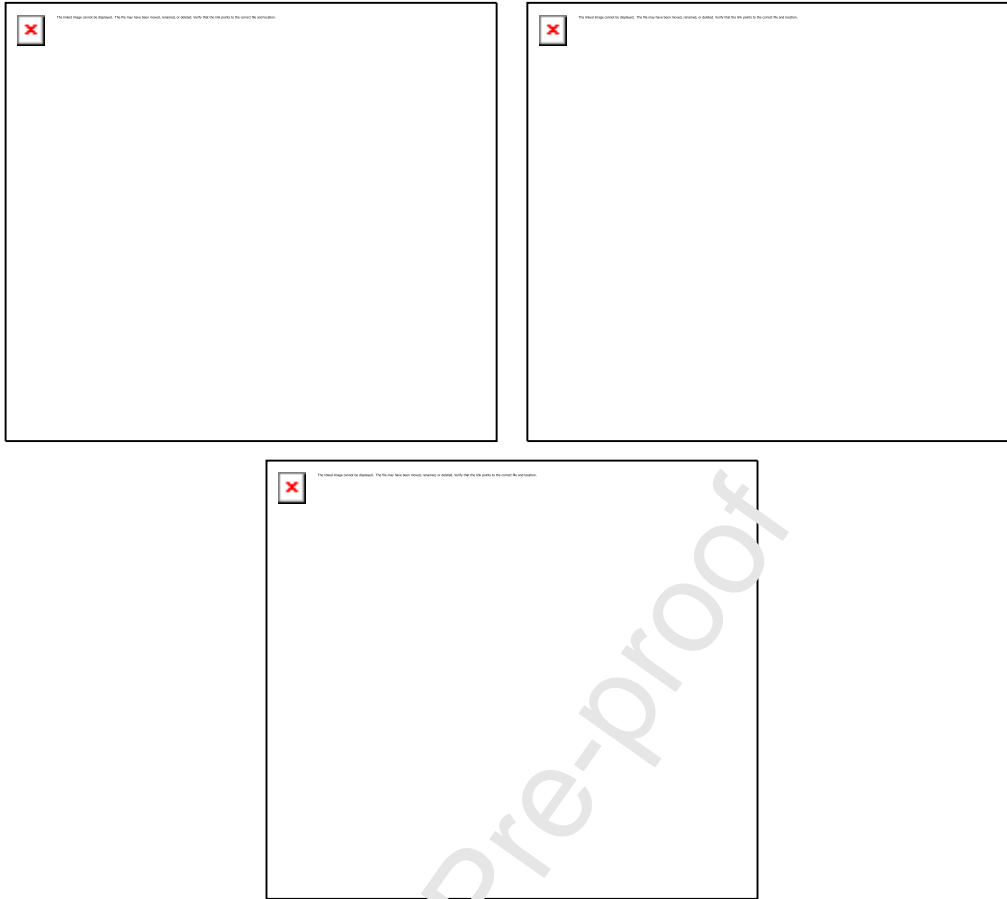
Fig.3. Spatial distributions of different surface parameters for typical zones of desertification

(Maduo County) (a) NDVI; (b) Albedo; (c) LST; (d) MSAVI; (e) TGSI.

3.2. Construction of monitoring model based on feature space

In this study, ten feature spaces were constructed using the 2D scatter plot tool in ENVI 5.3

with the five typical surface parameters described above (Figure 4). By analyzing the distribution

characteristics of different point clusters that corresponded to levels of desertification in feature

spaces, it could be found that the distance between any point (red point) to the certain point

(blue point) in the feature space (such as Albedo-MSAVI feature space) could distinguish different

levels of desertification, and the distance between any point (red point) to the certain line (blue

line) in the feature space (such as Albedo-LST feature space) could better identify the

desertification conditions. According to the above rules, ten feature spaces could be divided into

two categories: point-to-point mode (MSAVI-TGSI, NDVI-TGSI, MSAVI-NDVI, TGSI-Albedo, LST-MSAVI, NDVI-Albedo, TGSI-LST, and LST-NDVI) and point-to-line mode (Albedo-LST, MSAVI-Albedo).
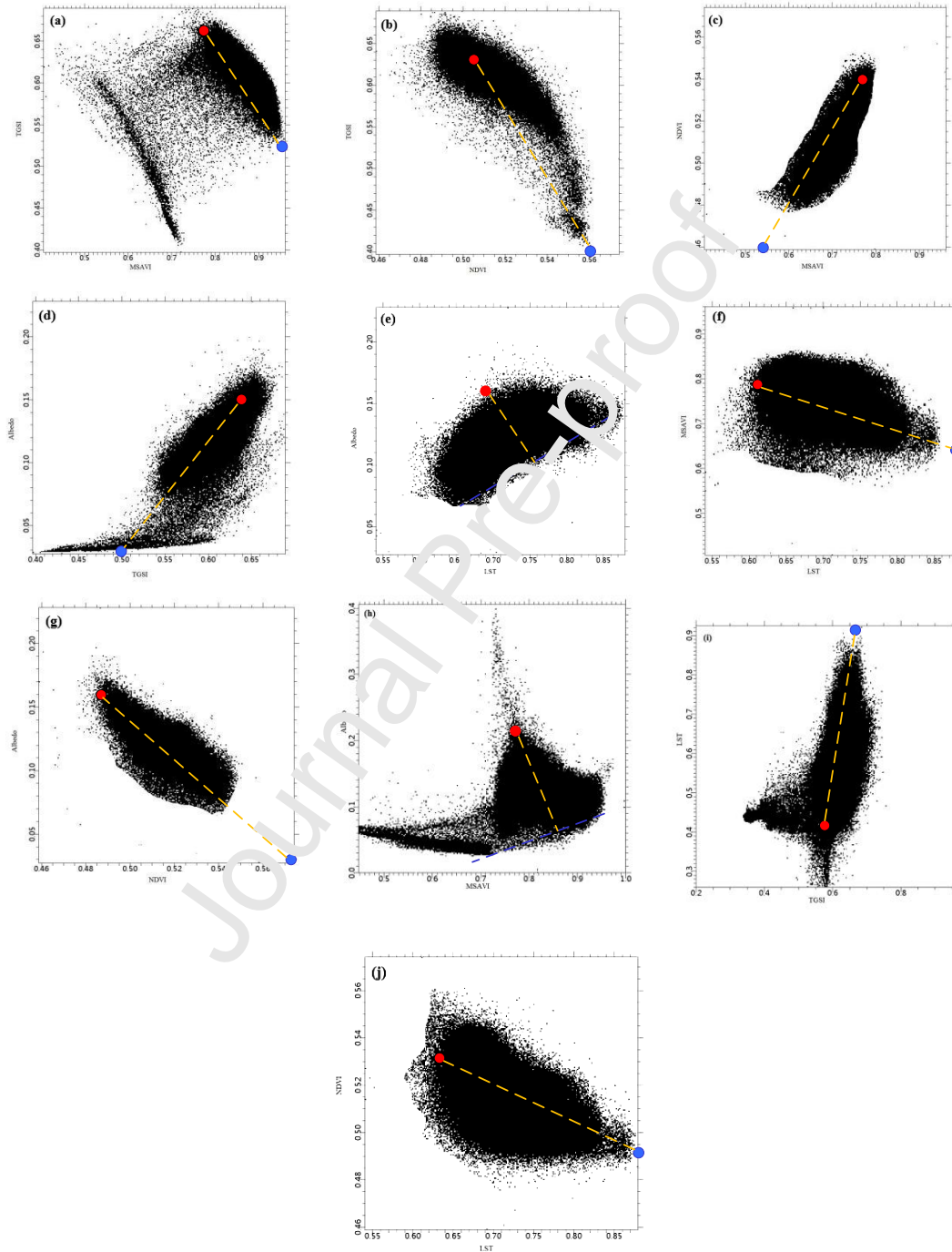

Fig.4. Ten typical feature spaces of desertification. (a) MSAVI-TGSI; (b) NDVI-TGSI; (c) MSAVI-NDVI;(d) TGSI-Albedo; (e) LST-Albedo; (f) LST-MSAVI; (g) NDVI-Albedo; (h) MSAVI-Albedo;

(i) TGSI-LST; (j) LST-NDVI.

For the point-to-point model, this study took LST-TGSI feature space as an example to analyze and construct the desertification monitoring model. Five point clusters were selected in the feature space to explore the spatial distribution law of different levels of desertification: Yellow, no desertification; Cyan, slight desertification; Green, moderate desertification; Blue, intensive desertification; Red, severe desertification. As shown in Fig.5, the LST increased with the enlarged TGSI. According to the distance from any point to point O (X_0, Y_0) in the feature space, the farther the distance from point O(X_0, Y_0), the more serious the desertification.
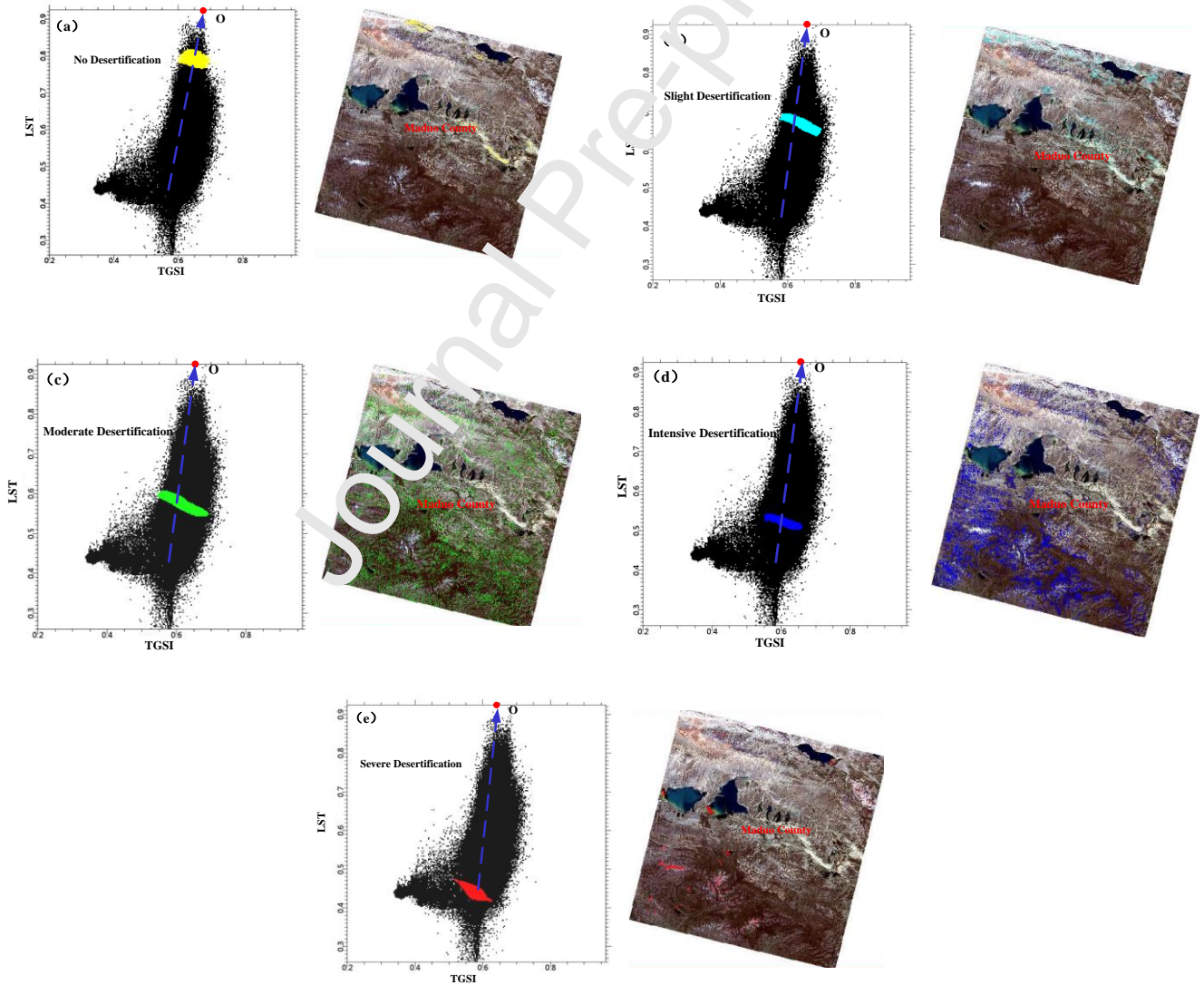
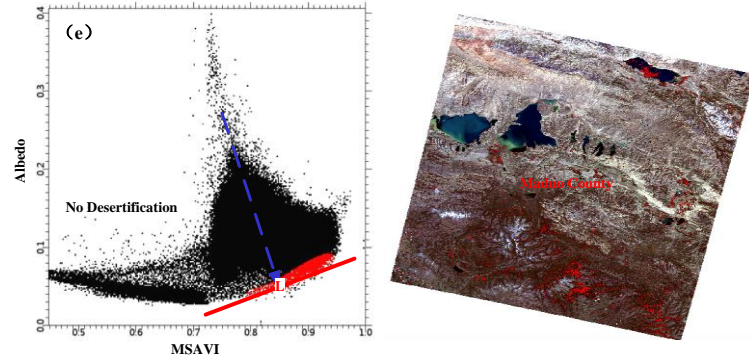**Fig.5.** Corresponding point clusters of different degrees of desertification in LST-TGSI feature

space for typical zones in Maduo County. (a) No Desertification; (b) Slight Desertification; (c)

Moderate Desertification; (d) Intensive Desertification; (e) Severe Desertification.

For the point-to-line model, Albedo-MSAVI was taken as an example in this study to analyze

and construct this category of model. Five point clusters were selected in the feature space to

explore the spatial distribution law of different levels of desertification: Yellow, severe

desertification; Cyan, intensive desertification; Blue, moderate desertification; Green, slight

desertification; Red, no desertification. There was an obviously negative linear correlation

between modified soil adjusted vegetation index and surface albedo. As shown in Fig.6, the

farther the distance between any point to the soil line (L) in the feature space, the more serious

the degree of desertification.
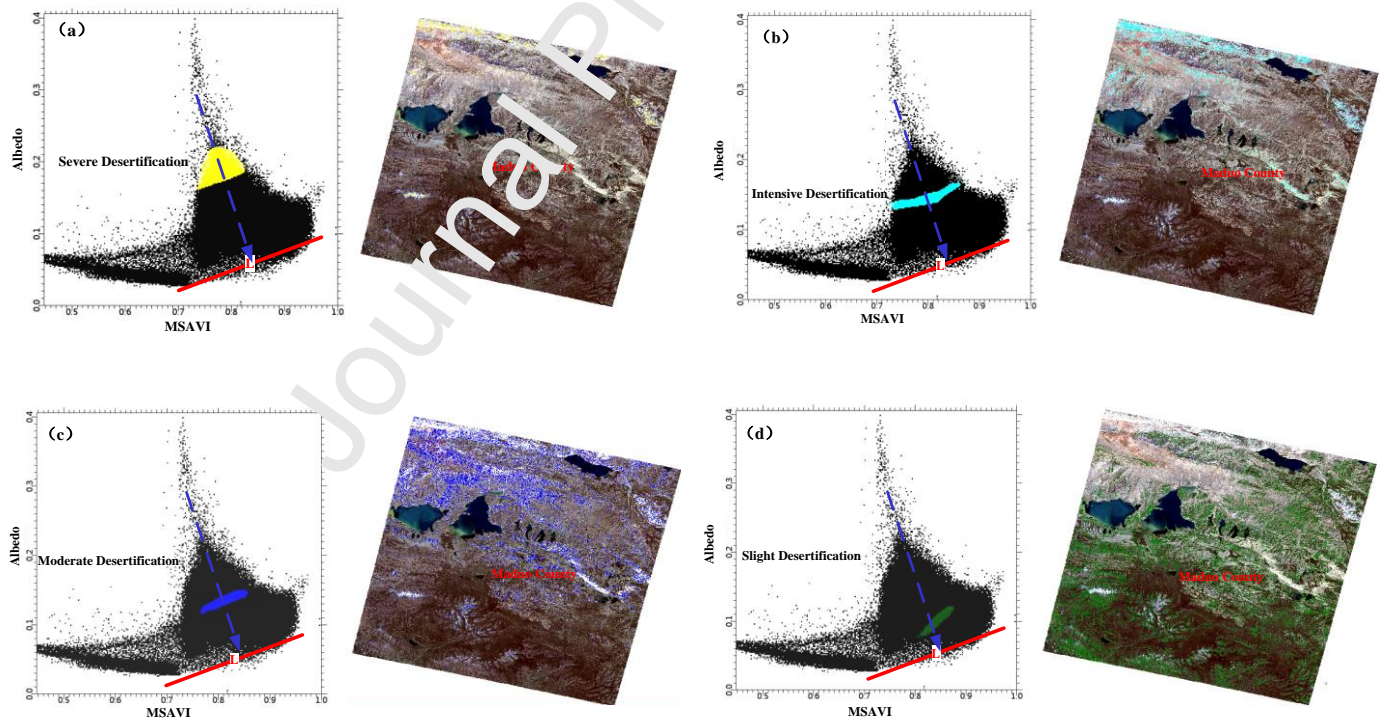
Fig.6. Corresponding point clusters of different degrees of desertification in Albedo-MSAVI

feature space for typical zones in Maduo County. (a) Severe Desertification; (b) Intensive

Desertification; (c) Moderate Desertification; (d) Slight Desertification; (e) No Desertification.

As indicated in Fig.7 (a), the farther the point clusters were from point C, the more serious

the desertification was. Different levels of desertification could be distinguished utilizing a line

perpendicular to CD. Therefore, the distance from any point D in the TGSI-LST feature space to

point O (M, N) can be utilized to distinguish the condition and evolution process of desertification,

its formula was as follows

$$LDMI_1 = \sqrt{(TGSI\text{-}M)^2 + (LST\text{-}N)^2} \qquad (12)$$

Where $LDMI_1$ is the desertification monitoring index.

As shown in Fig.7 (b), in the direction that perpendicular to the L line (soil line), the

Albedo-MSAVI feature space could be divided into several sections, which could effectively

distinguish different levels of desertification (Wu et al., 2013). According to the point to line

distance formula, the desertification remote sensing monitoring index model can be obtained as

follows:

$$Albedo = k \times MSAVI + b \qquad (13)$$

$$\mathrm{LDMI}_2 = \frac{|k \times \mathrm{MSAVI\text{-}Albedo} + b|}{\sqrt{1+k^2}} \tag{14}$$

Where LDMI$_2$ represents the desertification monitoring index, k represents the gradient of
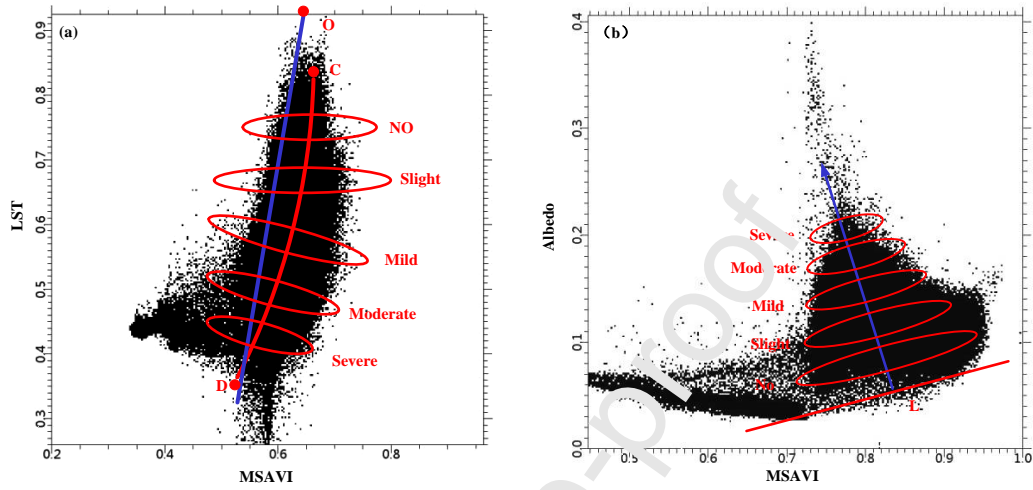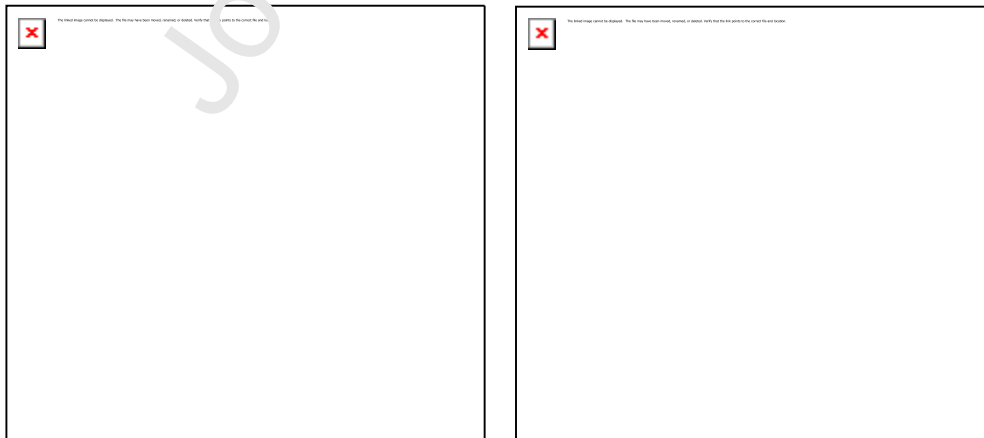
the soil line.

Fig.7. Construction of feature space model (a) Point-to-point model (LST-TGSI feature space); (b)

Point-to-line model (Albedo-MSAVI).

3.3. Precision validation

Based on the above two monitoring models, ten rocky desertification monitoring indices for

typical zones of desertification in Maduo County were calculated using ArcGIS 10.2(Fig.8).

Fig.8. Spatial distributions of desertification based on different feature space models. Point-to

-point model: (a) MSAVI-TGSI; (b) NDVI-TGSI; (c) MSAVI-NDVI; (d) TGSI-Albedo; (e) LST-MSAVI; (f)

NDVI-Albedo; (g) TGSI-LST; (h) LST-NDVI.   Point-to-Line model: (i) Albedo-LST; (j) MSAVI-Albedo

Maduo County was located in the western part of the source region of Yellow river, and its

climate was characterized by scare precipitation and strong evapotranspiration. Desertification

and sparse vegetation area were widely distributed in this County, where different levels of

densification occurred in the north and east parts. Therefore, Maduo County had the most typical

desertification phenomena over the whole study area. In this study, 144 verification samples

(30m×30m) were set using Google Earth from different land use types to confirm the spatial

uniformity and typicality of the selected samples. Then, the visual interpretation method was

applied to determine the actual desertification levels combined with some field observed data.

Finally, actual desertification information was utilized to evaluate and compare the applicability

of ten remote sensing monitoring indexes of desertification. In this paper, the precision index and

the basic error matrices (Table 1; formulas(15)-(18); Kong et al., 2012; Shi et al., 2018) were

adopted to test the accuracy of the inversion results.

$$C_{i+} = \sum_{j=1}^{n} C_{ij} \tag{15}$$

$$C_{+j} = \sum_{i=1}^{n} C_{ij} \tag{16}$$

$$P_{u,i} = C_{ii} / C_{i+} \tag{17}$$

$$P_{A,j} = C_{jj} / C_{+j} \tag{18}$$

where $P_{u,i}$ refers to the user accuracy of inversion category i, $P_{A,j}$ refers to the cartographic

accuracy of field observed category j , n represents the number of categories, C_{i+} represents the

sum of the inversion category i, C_{+j} represents the sum of field observed category j, and C_{ij} represents the number of the inversion category i, and field observed category j that both occur.

Table1. Basin error matrices of different levels of desertification (Taking point-to-point MSAVI-TGSI feature space model as an example)

	Desertification levels	NO	Slight	Moderate	Intensive	Severe	Total
	NO	**30**	2	0	1	0	33
	Slight	2	**40**	2	2	0	46
MSAVI-TGSI	Moderate	1	2	**36**	0	0	39
	Intensive	1	0	2	**13**	1	17
	Severe	0	0	0	2	**7**	9
	Total	34	44	40	18	8	**144**

The overall precision of the point-to-point MSAVI-TGSI feature space model is 87.5%, which is the ratio of the sum of correct verification points at each level (126) and total verification points (144). As shown in Table 2, the analysis results show that the accuracy of the desertification monitoring index based on the point-to-point Albedo-NDVI feature space model is the highest, with an overall precision of 88.4 %.

Table 2 Accuracy Comparison of Monitoring Index Based on Feature Space Models

Type of Model	Feature Space	Cartographic Accuracy
Point-to-Point	Albedo-MSAVI	81.2%
	MSAVI-LST	87.4%
	LST-NDVI	70.2%

	MSAVI-TGSI	87.5%
	LST-MSAVI	61.4%
	Albedo-MSAVI	76.4%
	LST-TGSI	52.3%
	Albedo-NDVI	88.4%
Point-to-Line	Albedo-LST	62.6%
	MSAVI-Albedo	75.6%

4. Desertification Monitoring in the Source Region of Yellow River

4.1. Spatial Distribution of Desertification during 1995-2015

Utilizing the optimal desertification monitoring index (Formulas (12)), with the tool of Raster Calculator of ArcGIS 10.2 with the point-to-point Albedo-NDVI feature space model, the desertification index in 1995, 2005, and 2015 was quantitatively calculated (Fig. 9). As shown in Table 3, the percentage of No Desertification area increased from 7.7 % to 17.9 % during 1995-2015, with an overall upward trend. The percentage of slight desertification area decreased from 39.2 % in 1995 to 31.8 % in 2005 and increased to 40.1 % in 2015. Meanwhile, the percentage of moderate desertification area rose from 30.2% in 1995 to 38.7% in 2005 and decreased to 31.8% in 2015. The percentage of the intensive desertification decreased from 21.1 % in 1995 to 9.1 % in 2015, showing an obvious downward trend. The percentage of severe desertification area decreased from 1.8 % in 1995 to 1 % in 2015. Furthermore, the percentage of desertification area in the study region has decreased over the last 20 years, from 92% in 1995 to 82.31% in 2015, indicating a downward trend overall with a decreased area of 12160.71 km^2. From 1990 to 2005, the desertification in the central region of the study area is relatively stable.

Moreover, the desertification in the eastern and southern parts has increased. After 2005, the

desertification in the upper reaches of the source region of Yellow River improved gradually, and

the desertification condition in northwestern Maduo county had been improved obviously.
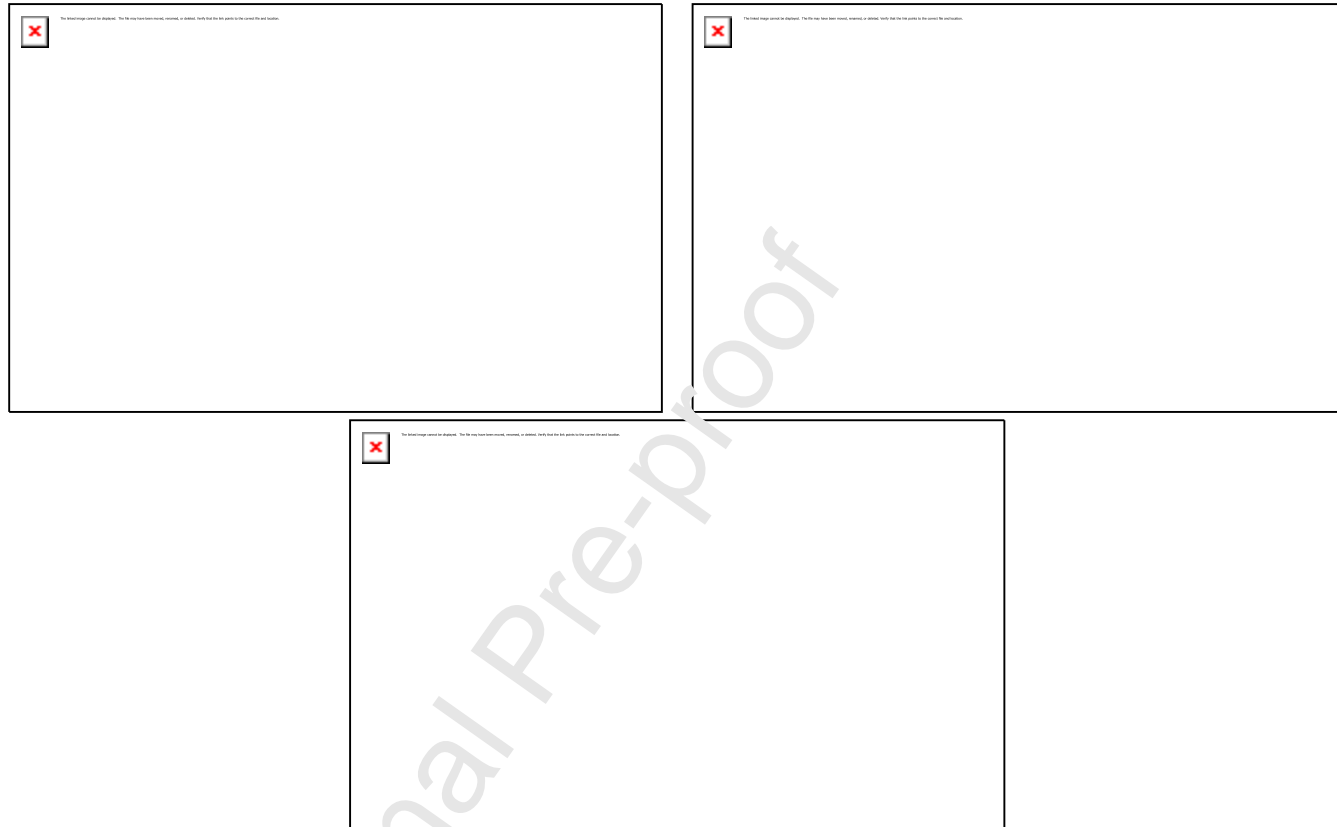
Fig.9. Spatial distribution of different levels of desertification in the source region of Yellow River.

(a) 1995; (b) 2005; (c) 2015

Table 3 Area and area percentage of different desertification levels from 1995 to 2015

Desertification levels	1995		2005		2015	
	Area(km^2)	Percentage(%)	Area(km^2)	Percentage(%)	Area(km^2)	Percentage(%)
No Desertification	9181.83	7.78	7120.71	6.04	21097.18	17.91
Slight desertification	46336.69	39.25	37453.57	31.79	47330.71	40.17
Moderate desertification	35517.23	30.08	45780.15	38.86	37444.86	31.78
Intensive desertification	24824.47	21.03	25600.08	21.73	10720.44	9.10

Severe desertification	2208.09	1.87	1849.06	1.57	1229.76	1.04

4.2. Changes in Desertification Intensity

In order to better show the spatial distribution of desertification change in the recent 20 years, the change intensity of desertification in different periods was calculated (Fig. 10). As shown in Fig.10, there is an overall improvement trend in desertification condition in the study area from 1995 to 2005. Zones of aggravated desertification were mainly concentrated in western Maduo county. In contrast, the zones of stable desertification are mainly located in the eastern and central regions. Meanwhile, zones of improvement desertification had the largest area of 43727.81 km^2. From 2005 to 2015, there was an obvious improvement in the desertification condition, especially in northwest parts of Maduo county. During 1995-2015, about 59 % of the desertification area had been improved, mainly concentrated in the northwest and east parts, while 7.5 % of the desertification area had aggravated, especially in northern Maduo county.
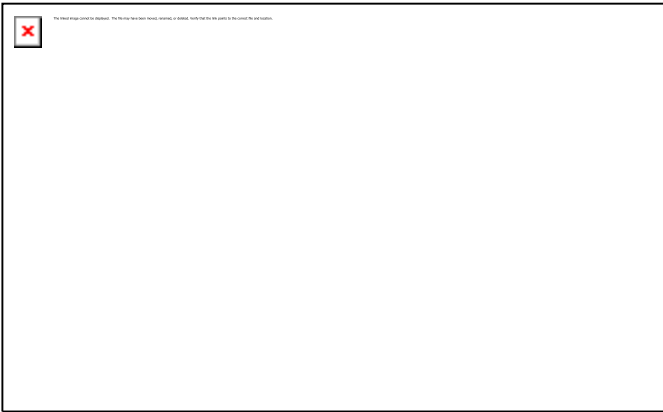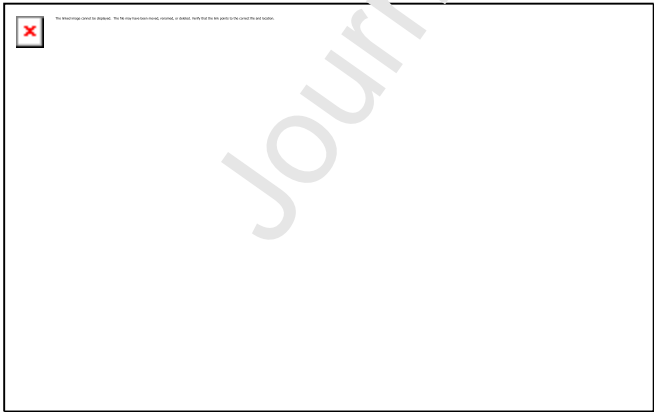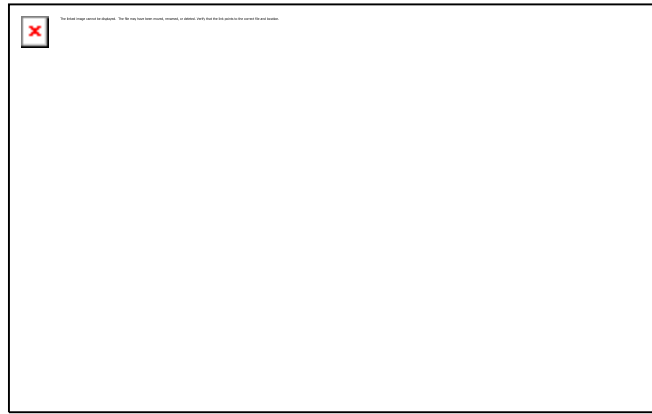
Fig.10. Change in Desertification Intensity in Different Periods (a) 1995-2005; (b) 2005-2015; (c)

1995-2015.

Table 4 Area comparisons of desertification intensity changes in different levels (Area/km^2)

Periods	Obvious Improvement	Improvement	Stable	Aggravation	Obvious Aggravation
1995-2005	11219.22	43727.81	3340.09	24784.73	3912.42
2005-2015	11644.08	89615.47	9410.85	4958.63	2071.32
1995-2015	16893.69	52276.80	39076.71	6308.23	2551.36

4.3. Spatial Distribution of Desertification in Different Vegetation Types

In order to analyze the relationships between different vegetation types and desertification,

five typical and most widely distributed vegetation types had been chosen to calculate with the

tool of Zonal Statistics of ArcGIS10.2. As shown in Fig. 11, except for the alpine grassland, the

other vegetation types in the study area were mainly dominated by slight desertification. Due to

the alpine grassland is in high altitude, where the temperature difference between day and night

was great and the precipitation was scare. Alpine grassland has the highest percentage of serious

desertification, up to 40%. In addition, compared with the alpine grassland, the alpine meadow

has more sufficient water conditions, thus the percentages of slight desertification area was

higher. Due to developed roots, strong regeneration ability, and better sand fixation ability of shrubs, the percentages of No Desertification area and slight desertification were the largest with 21 % (deciduous shrubs) and 55 % (shrubs), respectively. Due to the high vegetation coverage and a reliable water-heat supply, the overall desertification condition of evergreen coniferous forest is relatively light.
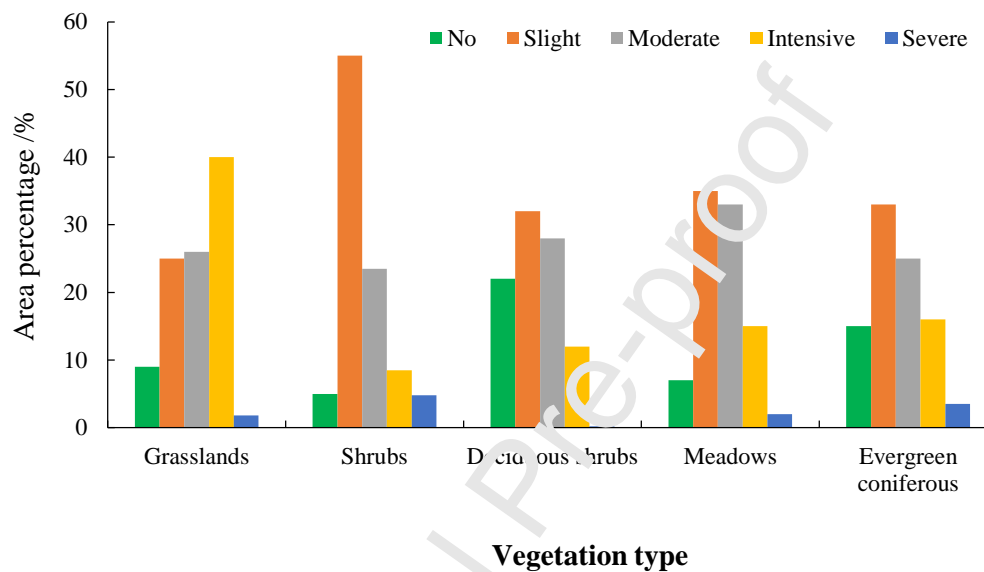
Fig.11. Area percentages of desertification levels with different vegetation types.

5. Factors influencing desertification in Source region of Yellow River

5.1. Single Factor

In this study, temperature, precipitation, land use, GDP, and population were selected as independent variables X, and the desertification index was selected as dependent variable Y. The influences of X on spatial differentiation of Y in 1995, 2005, and 2015 were calculated and analyzed by Geodetector (Formulas (1)-(4)). In addition, the influence or explanatory power of factor X on factor Y can be measured by q value.

As shown in Fig. 12, the q values of natural and human factors on desertification in 1995 was precipitation > GDP > population density > temperature > land use. The q value of precipitation

was the largest with 0.21, which was the dominant natural factor affecting desertification. Furthermore, among human factors, the q value of GDP density was the largest (0.16), followed by population density (0.12). Although temperature and land use affect desertification's spatial and temporal distribution, both the q values were small, only 0.1. Between 1995 and 2005, the explanatory power of population density continued to outperform that of GDP density and other natural factors, and its q value rose to 0.34, making it the dominating factor influencing desertification changes. The q value of natural and human factors affecting desertification was ranked as population density > GDP density > land use > precipitation > temperature. Precipitation was still the dominating natural factor causing desertification with a q value of 0.21. From 2005 to 2015, the q value of temperature rose to 0.16, surpassing precipitation and human factors and becoming the most critical element determining the desertification index. The q value of natural and human factors affecting desertification was ranked as temperature > population density > GDP density > land use > precipitation. The q value of population density was 0.1, which had the largest explanatory power in the human activity factors.
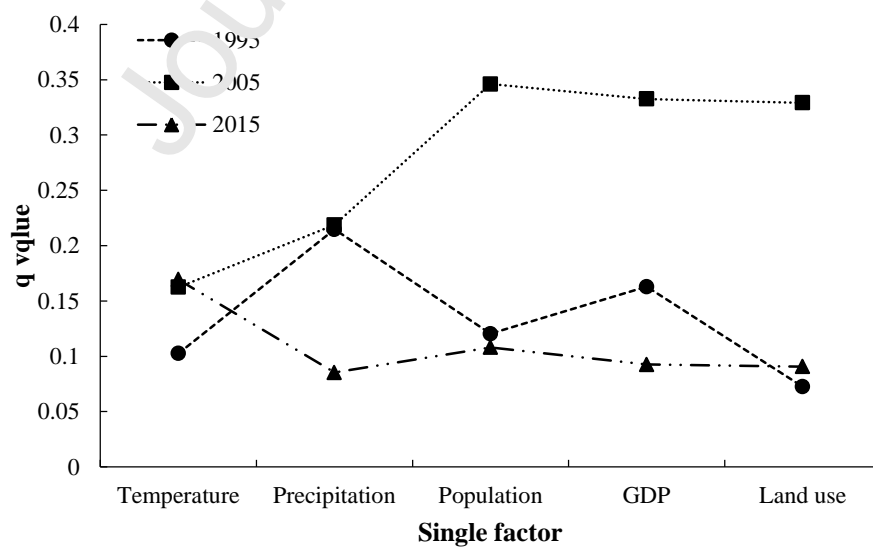
Fig.12. Comparisons of q value for different factors (1995, 2005, and 2015).

5.2. Interactive Factors

As shown in Fig.13, in 1995, all the factors showed nonlinear enhancement, and the interaction between different driving factors was analyzed by interaction factor detector (P<0.01). The explanatory power of the interactions of different factors was larger than that of the single factor. The orders of interactive factors were temperature ∩ precipitation > temperature ∩ population intensity > temperature ∩ GDP intensity > population intensity ∩ precipitation > precipitation ∩ GDP intensity > land use ∩ temperature > precipitation ∩ land use > GDP intensity ∩ land use > population intensity ∩ land use. The nonlinear enhancement was mainly concentrated in the interaction of natural factors in the nonlinear enhancement. The q value of precipitation ∩ temperature was the largest with 0.74, followed by temperature ∩ population intensity and temperature ∩ GDP intensity. The land use ∩ population intensity and land use ∩ GDP intensity had smaller q values of 0.33 and 0.42, respectively.
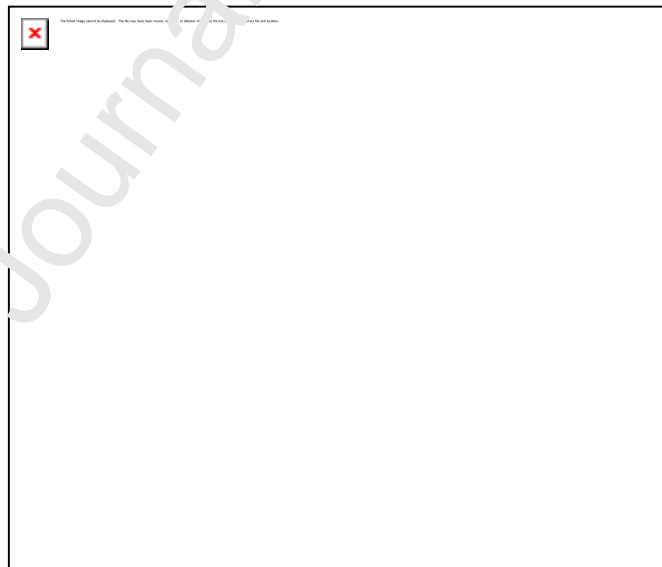
Fig.13. The q values of interactive factors in 1995 (P<0.01)

As shown in Fig.14, in 2005, the interactive factors of population intensity ∩ GDP intensity, population intensity ∩ land use , and GDP intensity ∩ land use showed bilinear enhancement,

and the rest showed nonlinear enhancement (P<0.01). The orders of interactive factors were as follows: GDP intensity ∩ precipitation > population intensity ∩ temperature > temperature ∩ precipitation> precipitation ∩ GDP intensity > population intensity∩ land use > GDP intensity ∩ temperature > precipitation ∩ land use > population intensity ∩ GDP intensity > land use ∩ GDP intensity. From 1995 to 2005, the interaction effects of human factors and natural factors were more obvious, and the q value of population intensity ∩ precipitation was 0.71. The natural interaction of temperature and precipitation was still an important indicator affecting the desertification index, with the q value of 0.61.
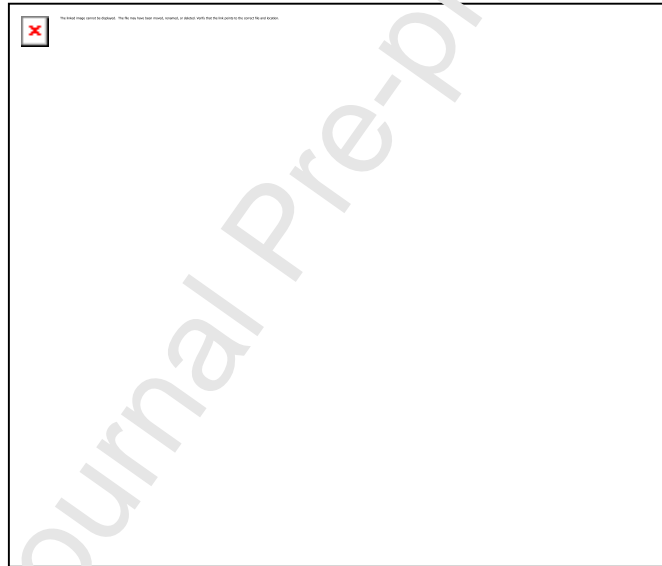
Fig.14. The q values of interactive factors in 2005 (P<0.01)

As shown in Fig.15, in 2015, all the interactive factors showed nonlinear enhancement (P<0.01), which were ranked as GDP intensity ∩ precipitation > temperature ∩ precipitation > population intensity ∩ precipitation > temperature ∩ GDP intensity > population intensity ∩ temperature > precipitation ∩ land use > land use ∩ temperature > population intensity ∩ land use > population intensity ∩ GDP intensity > land use ∩ GDP intensity. The q values of GDP intensity ∩ precipitation and temperature and population intensity ∩ precipitation were

larger than that of others. Therefore, the unreasonable development and utilization of the land

by human beings and livestock farming had obvious effects on land desertification in the study

region.

Fig.15. The q values of interactive factors in 2015 (P<0.01)

6. Discussions

6.1. Advantages of the proposed novel model

The evolution process of desertification was comprehensively influenced by natural factors

and human activities (Zhang et al., 2021). However, most previous studies utilized single indices

method (such as NDVI, MSAVI, TGSI) to indicate and monitor the desertification condition, which

could not obtain the desertification information with high precision, especially in zones

comprehensively affected by natural factors and human activities (Meng et al., 2021). In addition,

some scholars also applied the composite index method to evaluate the regional desertification

condition, which exaggerated the influences of some factors on desertification and ignored the

interactions among different evaluating factors (Sharma et al., 2021). Moreover, the image

classification method could better determine the desertification scope, however, it could not

obtain the spatial distribution of quantitative desertification information (Ahmed et al., 2022).

The feature space model that composed of two typical indices could better demonstrate the interactive relationship in 2-D feature space (Ye et al., 2018). In this paper, the novel desertification monitoring index based on feature space model provided a new approach for obtaining quantitative desertification information, and its average overall accuracy was more than 74.0 %. The proposed model above fully considered the complex and interactive influences of different surface parameters on the desertification process (Chen et al., 2021). Based on the point-to-point Albedo-NDVI feature space model, the remote sensing monitoring index has good applicability to detect the desertification condition, with an accuracy of 88.4 %, which had higher inversion accuracy than the proposed models of Fan and Qin, (2010) and Wu et al. (2019), with an accuracy of 82.0% and 75.9%, respectively. The reason is that NDVI could better indicate the surface vegetation growth and vegetation coverage information (Yang et al., 2007; Wu et al., 2019). In desertification zones, the above ground vegetation could effectively intercept suspended particles in aeolian sand flow and form sedimentation (Feng et al., 2021). Then, the underground plant roots would fix the sand particle to restrain the development of desertification (Wang et al., 2020). The sparser the surface vegetation distribution and the lower the NDVI, the more severe the desertification. Surface albedo is an important indicator of the radiation characteristics of the plant's underlying surface, which determines the amount of radiation absorbed by the underlying surface (Zhang et al., 2018). Surface conditions, such as vegetation cover, soil water content, snow cover would affect the change in Albedo value (Tang et al., 2001; Zhang et al., 2011). The combined utilization of the two above surface parameters could better reflect the evolution process of desertification than single indices. However, there is

a nonlinear relationship between Albedo and NDVI (as shown in Fig.4 (g)). Therefore, comprehensive method would not consider the interactions of the above two factors on desertification.

In addition, the inversion accuracy of monitoring indexes of point-to-point MSAVI-LST and MSAVI-TGSI feature space model is also high, with 87.4 % and 87.5 %, respectively. The main reason is that MSAVI could consider the bare soil line and increased the dynamic range of vegetation information, which would eliminate the influence of soil background on vegetation index, and could better reflect the vegetation condition in low coverage areas (Yan et al., 2009). In addition, bare land or low vegetation coverage is widely distributed in the middle and west of the source region of Yellow River. The bare land or sand has smaller heat capacity than water or vegetation (Sun et al., 2019). The surface temperature of bare land would be higher than that of fully covered land under the same imaging conditions. Therefore, LST is also a useful indicator of desertification (Guo et al., 2020a). Meanwhile, topsoil grain size index could better reflect the sand content percentage of topsoil. With the aggravation of the desertification, the particle size of the topsoil would become rougher and the content percentage of sand became larger (Zhang and Jin, 2021). Thus, TGSI is also a better indicator to reflect the conditions and changes of desertification. Based on remote sensing, the combination of MSAVI, LST, and TGSI would enhance the inversion accuracy of desertification monitoring. Wei et al. (2018) had utilized the MSAVI, LST, and TGSI to establish the feature space models of Albedo-NDVI, Albedo-MSAVI, and Albedo-TGSI to monitor the desertification condition of the Mongolian plateau. However, these above proposed models had ignored the non-linear relationships among MSAVI, LST, and TGSI, which caused lower overall inversion accuracy (84.5%, 85.6, and 88.2) than that of our

investigation. Moreover, Wu et al. (2019) had directly applied the Albedo and MSAVI to monitor the desertification of Shengli mining area, which did not consider the applicability of indicators, and its overall precision was 75.9%.

Due to the fact that the desertification inversion accuracy of the feature space model depended on the accurate calculation of typical surface parameters, it is necessary to select the optimal images with appropriate observation time according to the land surface cover types (Zheng et al., 2018). The average inversion accuracy of the models based on images in growing season (75.3%) were higher than that of images in spring(55.3%) and winter (60.1%)(Guo et al.,2020a). In addition, the spatial distributions of impervious surface in some feature spaces (such as MSAVI-LST and Albedo-LST) are similar, which would reduce the inversion accuracy of desertification information. The inversion accuracy of the above two feature space model would be improved by 16.8% when the impervious surface such as residential area, industrial and mining land had been removed (Wei et al., 2018).

6.2. Dominant driving factors of the desertification changes during different periods

The desertification condition of the source region of Yellow River belonged to moderate level, which is the result of comprehensive actions of climate change and human activities (Shen et al., 2018). Zones with intensive and severe desertification are mainly distributed in Qumalai and Maduo and it is due to the fact that the climate is characterized by scare precipitation, larger dryness and strong wind, which lead to widely distributed bare land or low vegetation coverage area (Kong et al., 2012). Meanwhile, the desertification of the junction zones of Gande-Dari-Jiuzhi -Banma is severe, which is consistent with the results of Zhang et al. (2018). The main reason is that unreasonable human activities, such as overgrazing, urbanization and excessive cultivated

land reclamation, cause the degradation of a large area of grassland (Zhang and Jin, 2021). During 1995-2005, the desertification condition shows an overall improvement in the study region, which is consistent with the investigation of Wang et al. (2020). This is due to effective implementation of the protection project and afforestation project of Sanjiangyuan, which obtained important achievements (Ye et al., 2018). The vegetation coverage is greatly improved and the biodiversity has also increased. Moreover, there is an increased trend of precipitation and the hydrothermal condition had been improved largely, which is conducive to the vegetation restoration.

With the increased disturbance intensity of climate change and human activity, the dominant influence factors of desertification evolution process has changed. However, most previous studies focused on the driving factor analysis of desertification for certain period, the change law of dominant influence factors was fewer reported (Guo et al., 2020b). For single factor analysis, from 1995 to 2005, natural factors were the dominant factors affecting the spatial distribution of desertification in the study region, followed by land use, GDP density, population density, and other human factors (Chen et al., 2021). During this period, increased precipitation and temperature had greatly contributed to the improvement of the desertification, while the human activity (such as overgrazing and urbanization) exacerbated the process of desertification to some extent (Yuan et al., 2015). After 2005, human activities had gradually weakened the dominant role of natural factors in the evolution process of desertification. There is an increasing trend of explanatory power of population intensity, GDP intensity, and land use. The implementation of the Sanjiangyuan Reigion protection project and afforestation project have greatly improved vegetation cover and ecological diversity.

However, the explanatory power of independent natural factor and human factor is weaker than that of the interaction among factors, which is consistent with the studies of Chen et al (2021).　The spatial distribution of desertification has formed by the combined effects of natural factors and human factors (Guo et al., 2020e). In 1995, the dominant interactive factor was temperature ∩ precipitation (0.74), followed by temperature ∩ population intensity(0.67) and temperature ∩ GDP intensity (0.66). In this period, temperature ∩ other factors play an important role in the evolution process of desertification. In 2005, the precipitation ∩ population intensity had the largest q value of 0.71, followed by that of temperature ∩ population intensity and temperature ∩ precipitation. Due to the implementations of the project of returning farmland to forest and grassland and the protection project of the Three-River Source Region, human activity gradually weaken the influences of climate factor (Li et al., 2011). However, the temperature and precipitation still greatly contribute to the desertification change. In 2015, the GDP intensity ∩ precipitation had the largest explanatory power of desertification evolution process, while that of population intensity ∩ precipitation and temperature ∩ GDP intensity was larger.　With the urbanization and implementations of ecological environment protection measures, human activity has become the dominant factors of desertification process.

7. Conclusions

Based on Landsat images, this paper proposed and constructed the optimal desertification monitoring index based on feature space. Then the evolution process of the desertification in the study region and its driving factors were analyzed. The main conclusions are as follows:

(1) The desertification monitoring index based on the feature space model has better application in obtaining desertification information on large-scale regions. The point-to-point

Albedo-NDVI model has the highest accuracy with 88.4 %, followed by that of the point-to-point

MSAVI-TGSI model with 87.5 %.

(2) From 1995 to 2015, the desertification showed an overall improvement trend. The

percentage of desertification areas decreased from 92 % in 1995 to 82.31 % in 2015.

(3) During 1995-2015, the desertification in the central part of the study region was

relatively stable, and the desertification condition in the eastern and southern parts showed an

aggravation trend. After 2005, the desertification condition showed an overall improvement

trend, especially in Maduo county.

(4) During 1995-2015, the natural factors were the dominant factors in influencing the

spatial distribution of desertification, but after 2005, human activities became the primary

factors that aggravated or improved the condition of desertification.

(5) The explanatory power of the interaction of natural factors and human factors on

desertification is larger than that of independent natural factors or human factors. During the

past twenty years, human activity had become the dominant factor in the evolution process of

desertification.

Based on feature space, a novel desertification monitoring index has been proposed to

reveal the spatial and temporal change law of desertification process. However, the physical

mechanism of the interactions among different factors is unclear. Moreover, the desertification

changes are comprehensively influenced by more than three natural or anthropogenic factors.

Therefore, the interactive relationships among three or more factors in 3D or n-D feature space

are urgent to explore in future studies.

Acknowledgement

References

Ahmed, S.A., Abdelatif, D.A., 2022. Assessment of desertification using modified MEDALUS model in the north Nile Delta, Egypt. Geoderma. 405, 115400. https://doi.org/10.1016/j.geoderma.2021.115400.

Chen, A., Yang, X.C., Guo, J., Xing, X.Y., Yang, D., Xu, B., 2021. Synthesized remote sensing-based desertification index reveals ecological restoration and its driving forces in the northern sand-prevention belt of China. Ecol. Indic. 131, 108230. https://doi.org/10.1016/J.ECOLIND.2021.108230.

Chen, S.T., Guo, B., Zhang, R., Zang, W.Q., Wei, C.X., Wu, H.W., Yang, X., Zhen, X.Y., Li, X., Zhang, D.F., Han, B.M., Zhang, H.L., 2021. Quantitatively determine the dominant driving factors of the spatial–temporal changes of vegetation NPP in the Hengduan Mountain area during 2000-2015. J. Mt. Sci-Engl. 18(2), 427-445. https://doi.org/10.1007/s11629-020- 6404-9.

Feng, J., Ding, J.L., Wei, W.Y., 2018. A study of soil salinization in Weigan and Kuqa Rivers Oasis based on Albedo-MSAVI feature space. China Rural Water and Hydropower. (02), 147-152. https://doi.org/10.11821/yj2013020003.

Feng, K., Wang, T., Liu, S.L., Yan, C.Z., Kang, W.P., Chen, X., Guo, Z.C., 2021. Path analysis model to identify and analyse the causes of aeolian desertification in Mu Us Sandy Land, China. Ecol.

Indic. 124, 107386. https://doi.org/10.1016/J.ECOLIND.2021.107386.

Guo, B., Zang, W.Q., Han, B.M., Yang, F., Luo, W., He, T.L., Fan, Y.W., Yang, X., Chen, S.T., 2020a. Dynamic monitoring of desertification in Naiman Banner based on feature space models with typical surface parameters derived from Landsat images. Land Degradation and Development. 31, 1573-1592. https://doi.org/10.1002/ldr.3533.

Guo, B., Zang, W.Q., Luo, W., 2020b. Spatial-temporal shifts of ecological vulnerability of Karst Mountain ecosystem-impacts of global change and anthropogenic interference. Sci. Total. Environ. 741, 140256. https://doi.org/10.1016/j.scitotenv.2020.140256.

Guo, B., Zang, W.Q., Luo, W., Wen, Y., Yang, F., Han, B.M., Fan, Y.W., Chen, X., Qi, Z., Wang, Z., Chen, S.T., Yang, X., 2020c. Detection model of soil salinization information in the Yellow River Delta based on feature space models with typical surface parameters derived from Landsat8 OLI image. Geomatics. Natural Hazards and Risk. 11(1), 288-300. https://doi.org/10.1080/19475705.2020.1721573.

Guo, B., Zang, W.Q., Yang, F., Han, B.M., Chen, S.T., Liu, Y., Yang, X., He, T.L., Chen, X., Liu, C.T., Gong, R., 2020e. Spatial and temporal change patterns of net primary productivity and its response to climate change in the Qinghai-Tibet Plateau of China from 2000 to 2015. J. Arid. Land. 12(1), 1-17. https://doi.org/10.1007/s40333-019-0070-1.

Guo, B., Zang, W.Q., Yang, X., Huang, X.Z., Zhang, R., Wu, H.W., Yang, L.A., Wang, Z., Sun, G.Q., Zhang, Y., 2020d. Improved evaluation method of the soil wind erosion intensity based on the cloud–AHP model under the stress of global climate change. Sci. Total. Environ. 746, 141271. https://doi.org/10.1016/j.scitotenv.2020.141271.

Huete, A.R., 1988. A soil-adjusted vegetation index. Remote. Sens. Environ. 25, 295-309.

https://doi.org/10.1016/0034-4257(88)90106-X.

Kong, B., Tao, H.P., Liu, B.T., 2012. Estimation model of freeze-thaw erosion in Western Sichuan Plateau. Disaster Adv. 5(4), 1287-1290.

Lamchin, M., Lee, J.Y., Lee, W.K., Lee, E.J., Kim, M., Lim, C.H., Choi, H.A., Kim, S.R., 2016. Assessment of land cover change and desertification using remote sensing technology in a local region of Mongolia. Adv. Space Res. 57, 64-77. https://doi.org/10.1016/j.asr.2015. 10.006.

Li, J.C., Yang, Y.G., Zhang, C.X., 2011. Quantitative study on influencing factors of desertification in headwater area of Yellow River. J. Arid. Land. Resour. Environ. 25(02), 88-92. https://doi.org/10.13448/j.cnki.jalre.2011.02.001.

Liu, Q.S., Liu, G.H., Huang, C., 2018. Monitoring desertification processes in Mongolian Plateau using MODIS tasseled cap transformation and TGSI time series. J. Arid. Land. 10(01), 12-26. https://doi.org/10.1007/s40333-017-0109-0.

Ma, Z.Y., 2013. Quantitative extraction method of desertification information based on TM image. Lanzhou University

Meng, X.Y., Gao, X., Li, S., Li, S.Y., Lei, J.Q., 2021. Monitoring desertification in Mongolia based on Landsat images and Google Earth Engine from 1990 to 2020. Ecol. Indic. 129, 107908. https://doi.org/10.1016/J.ECOLIND.2021.107908.

Pan, J.H., Qin, X.J., 2010. Extracting desertification from landsat imagery using a feature space composed of vegetation index and albedo-a case study of Zhangye oasis and its adjacent areas. Science of surveying and mapping. 35(3), 193-195. https://doi.org/10.16251/j.cnki. 1009-2307.2010.03.036.

Ren, Y.Q., Liu, H.L., Tang, L.X., Jang, L.L., An, X.Y., 2014. A study on dynamic changes of desertification in south edge of Junggar Basin based on NDVI-Albedo features. Bull. Soil. Water. Conserv. 34(02), 267-271. https://doi.org/10.13961/j.cnki.stbctb.2014.02.055.

Sharma, L.K., Raj, A., Somawat, K., 2021. Spatio-temporal assessment of Environmentally Sensitive Areas (ESA) in The Thar Desert India, to combat desertification under UNCCD framework. J. Arid. Environ. 194, 104609. https://doi.org/10.1016/J.JARIDENV.2021.104609.

Shen, X.J., An, R., Feng, L., Ye, N., Zhu, L.J., Li, M.H., 2018. Vegetation changes in the Three-River Headwaters Region of the Tibetan Plateau of China. Ecol. Indic. 93, 804-812. https://doi.org/10.1016/j.ecolind.2018.05.065.

Shi, S.E., Wei, W., Yang, D., Hu, X., Zhou, J.J., Zhang, Q., 2018. Spatial and temporal evolution of eco-environmental quality in the oasis of Shiyang River Basin based on RSEDI. Chinese. J. Ecol. 37(04), 1152-1163. https://doi.org/10.13292/j.1000-4890.201804.034.

Sun, J., Hou, G., Liu, M., Fu, C., Zhan, T.Y., Zhou, H.K., Tsunekawa, A., Haregeweyn, N., 2019. Effects of climatic and grazing changes on desertification of alpine grasslands, Northern Tibet. Ecol. Indic. 107, 105647. https://doi.org/10.1016/j.ecolind.2019.105647.

Tang, S.H., Zhu, Q.J., Yan, G.J., 2001. Theories and methods of terrestrial parameter extraction from remote sensing. J. Beijing Normal University (Natural Science). 37(2), 266-273.

Wang, J.F., Xu, C.D., 2017. Geodetector: Principle and prospective. Acta. Geogr. Sin. 72(01), 116-134. https://doi.org/10.11821/dlxb201701010.

Wang, L.Y., Wu, Q.B., Jiang, G.L., 2020. The effect of desertification on frozen soil on the Qinghai-Tibet plateau. Sci. Total. Environ. 711, 134640. https://doi.org/10.1016/j.scitotenv.

2019.134640.

Wang, Z.X., Jiang, Y.J., Zhang, Y.Z., Duan, S.H., Liu, J.C., Zeng, Z., Zeng, S.B., 2019. Spatial

distribution and driving factors of karst rocky desertification based on GIS and geodetectors.

Acta. Geogr. Sin. 74(05), 1025-1039. https://doi.org/10.11821/dlxb201905014.

Wei, H.S.,Wang, J.L., Cheng, K., Li, G., Ochir, A., Davaasuren,D., Chonokhuu, S., 2018.

Desertification Information Extraction Based on Feature Space Combinations on the

Mongolian Plateau Remote.Sens. 10, 1614. https://doi.org/10.3390/rs10101614.

Wen, Y., Guo B., Zang, W.Q., Ge, D.Z., Luo, W., Zhao, H.H., 2020. Desertification detection model

in Naiman Banner based on the albedo-modified soil adjusted vegetation index feature

space using the Landsat8 OLI images. Geomatics. Natural Hazards and Risk. 11(1), 544-558.

https://doi.org/10.1080/19475705.2020.1734100.

Wu, H.F., Chen, Z.Q., 2019. Transfer matrix and buffer of the urban heat island effect in Fuzhou. J.

Tianjin Normal University (Natural Science Edition). 39(03), 69-75. https://doi.org/

10.19638/j.issn1671-1114.20190312.

Wu, H.W., Guo, B., Fan, J.F., Yang, F., Han, B.M., Wei, C.X., Lu, Y.F., Zang, W.Q., Zhen, X.Y., Meng, C.,

2021. A novel remote sensing ecological vulnerability index on large scale: A case study of

the China-Pakistan Economic Corridor region. Ecol. Indic. 129, 107955.https:// doi.org

/10.1016/J.ECOLIND.2021.107955.

Wu,Z.H., Lei, S.G., Bian, Z.F., Huang, J., Zhang, Y.,2019. Study of the desertification index based on

the albedo-MSAVI feature space for semi-arid steppe region. Environ. Earth. Sci. 78,232.

https://doi.org/10.1007/s12665-019-8111-9.

Wu, Z.H., Li, T., 2013. The comprehensive performance evaluation of the High-tech Development

Zone: Analysis based on the natural breakpoint method. Statistics and Inform. Forum. 28(03), 82-88. https://doi.org/10.3969/j.issn.1007-3116.2013.03.014.

Yan, C.Z., Song, X., Zhou, Y.M., Duan, H.C., Li, S., 2009. Assessment of aeolian desertification trends from 1975's to 2005's in the watershed of the Longyangxia Reservoir in the upper reaches of China's Yellow River. Geomorphology. 112(3-4), 205-211.

Yang, G.J., Liu, Q.H., Liu, Q., Gu, X.F., 2007. Estimating subpixel surface temperature coupling retrieval land surface parameters with GA-SOFM neural network. Acta. Sci. Naturalium. U. Pekinensis. 43(4), 484-492. https://doi.org/10.13209/j.0479-8023.2007.079.

Ye, H., Zhang, Y.B., Yi, G.H., Li, J.J., Bie, X.J., Liu, D., Luo, J.L., 2018. Spatio-temporal characteristics of evapotranspiration and its relationship with climate factors in the source region of Yellow River from 2000 to 2014. Acta. Geogr. Sin. 73(11), 2117-2134. https://doi.org/10.11821/dlxb201811006.

Yuan, F.F., Berndtsson, R., Zhang, L., Uvo, C.B., Hao, Z.C., Wang, X.P., Yasuda, H., 2015. Hydro climatic trend and periodicity for the source region of Yellow River. J. Hydrol Eng. 20(10), 05015003. https://doi.org/10.1061/(ASCE)HE.1943-5584.0001182.

Zeng, Y.N., Feng, Z.D., 2007. Spatial and temporal changes of desertification in the headwater area of the Yellow River using remote sensing. Acta. Geogr. Sin. 62(05), 529-536.

Zeng, Y.N., Feng, Z.D., Xiang, N.P., 2005. The remote sensing synthetic index model for desertification detection. Remote. Sens. Land and Resour. (02), 40-44.

Zeng, Y.N., Xiang, N.P., Feng, Z.D., Xu, H., 2006. Albedo-NDVI space and remote sensing synthesis index models for desertification monitoring. Sci. Geogr. Sin. 26(01), 75-81.

Zhang, C.L., Li, Q., Shen, Y.P., Zhou, N., Wang, X.S., Li, J., Jia, W.R., 2018. Monitoring of aeolian

desertification on the Qinghai-Tibet Plateau from the 1970s to 2015 using Landsat images. Sci. Total. Environ. 619-620, 1648-1659. https://doi.org/10.1016/j.scitotenv. 2017.10. 137.

Zhang, C.X., Wang, X.M., Li, J.C., Zhang, Z.C., Zheng, Y., 2021. The impact of climate change on aeolian desertification in northern China: Assessment using aridity index. Catena. 207, 105681. https://doi.org/10.1016/J.CATENA.2021.105681.

Zhang, X.C., Jin, X.M., 2021. Vegetation dynamics and responses to climate change and anthropogenic activities in the Three-River Headwaters Region, China. Ecol. Indic. 131, 108223. https://doi.org/10.1016/J.ECOLIND.2021.108223.

Zhang, X.Z., Zheng, J.Y., He, F.N., Wang, Z.S., 2011. Application of MODIS BRDF/Albedo dataset in the regional temperature simulation of China. Acta. Geogr. Sin. 66(3), 356-366.

Zhang, Z.W., Chang, T.Y., Gao, X., 2021. Analysis of Eco-economic Coordination of Yellow River Basin. Areal. Res. Dev. 40(2), 25-30, 36. https://doi.org/10.3969/j.issn.1003-2363. 2021.03.005.

Zhao, C.Z., Jia, L.H., 2009. Ecological performance and sustainable problems with the grazing forbidden project in the resource regions of the Yellow River. J. Lanzhou university (Natural sciences). 45(01), 37-41. https://doi.org/10.13885/j.issn.0455-2059.2009.01.023.

Zheng, Y.T., Han, J.C., Huang, Y.F., Steven, R.F., Xie, S., Lv, E.Z., Chen, M., 2018. Vegetation response to climate conditions based on NDVI simulations using stepwise cluster analysis for the Three-River Headwaters region of China. Ecol. Indic. 92, 18-29. https://doi.org/10.1016/j.ecolind.2017.06.040.

Zhu, X., Yang, Y.B., Li, X.L., Zhang, X.Z., Shan, L.L., 2018. Research on Landsat 8 surface temperature inversion algorithm. Geospatial. Inform. 16(09), 103-106. https://doi.org/

Author contributions statement

Bing Guo: Conceptualization, Methodology, Software，Data curation, Writing-Original draft preparation

Cuixia Wei，Yang Yu：Funding Acquisition, Supervision, Project Administration

Yifeng Liu, Jialin Li: Resources, Investigation, Revision.

Chao Meng，Yumei Cai: Methodology, Software，Data curation.

Declaration of interests

☐The authors declare that they have no known competing financial interests or personal relationships that could have appeared to influence the work reported in this paper.

☒The authors declare the following financial interests/personal relationships which may be considered as potential competing interests:

Bing Guo reports writing assistance was provided by Chinese Academy of Sciences. Bing Guo reports a relationship with Chinese Academy of Sciences that includes: non-financial support. Bing Guo has patent pending to licensee. null

Graphical abstract

Typical land surface paramters

Establishment of desertification index model

Construction of feature space

Point to point model

$$LDMI_1 = \sqrt{(TGSI\text{-}M)^2 + (LST\text{-}N)^2}$$

Optimal monitoring model of desertification

Verification

Point to line model

Albedo=$k \times$MSAVI+b

$$LDMI_2 = \frac{|k \times MSAVI\text{-}Albedo+b|}{\sqrt{1+k^2}}$$

Driving factor

Climate change Human activity

Distinguish the effects of Climate-human activity

Change process of desertification

Dominant single factor

Geodetector

Dominant interactive factor

Population intensity ∩ Temperature（1995） → Population intensity ∩ Precipitation（2005） → GDP intensity ∩ Precipitation（2015）

Spatial-temporal change patterns

Deterging the dominant factor

Highlights

1. A novel remote sensing monitoring index of desertification based on feature space model has been proposed;

2. The point-to-point Albedo-NDVI feature space model has the best inversion precision of 88.4 %;

3. Human disturbance had gradually become the dominant factors;

4. The explanatory power of the interaction of natural factors and human factors was greater than that of any individual one.